Biosensors and Bioelectronics 131 (2019) 207–213

Contents lists available at ScienceDirect

Biosensors and Bioelectronics

journal homepage: www.elsevier.com/locate/bios

Dandelion-like CuO microspheres decorated with Au nanoparticle modified biosensor for Hg^{2+} detection using a T-Hg^{2+}-T triggered hybridization chain reaction amplification strategy

Yujie Yu[a,b,1], Chao Yu[c,1], Rufei Gao[a,b], Jun Chen[c], Hangtian Zhong[a,b], Yilin Wen[c], Xingduo Ji[a,b], Jiahao Wu[a,b], Junlin He[a,b,*]

[a] School of Public Health and Management, Chongqing Medical University, Chongqing, China
[b] Joint International Research Laboratory of Reproduction & Development, Chongqing Medical University, Chongqing, China
[c] College of Pharmacy, Chongqing Medical University, Chongqing, China

ARTICLE INFO

Keywords:
Hg^{2+} detection
Dandelion-like CuO
Thymine-Hg^{2+}-thymine
Hybridization chain reaction
Toluidine blue

ABSTRACT

We fabricate a novel electrochemical biosensor based on the specific thymine-Hg^{2+}-thymine (T-Hg^{2+}-T) base pair for the highly sensitive detection of mercury ions (Hg^{2+}) and utilize toluidine blue (TB) as a redox indicator that is combined with a hybridization chain reaction (HCR) for signal amplification. The dandelion-like CuO (D-CuO) microspheres that were assembled using Au nanoparticles were first introduced as support materials, which produced more active sites for the thiolated probe (P1) combination. Then, the presence of Hg^{2+} induced P1 to hybridize with the other oligonucleotide (P2) through Hg^{2+}-mediated T-Hg^{2+}-T complexes. In addition, the partial sequence of P2 acted as an initiator sequence, which led the two hairpin DNA (H1 and H2) strands to collectively form the extended double-strand DNA through the HCR process on the electrode surface. TB was employed to interact with the double strands and produce an efficient electrochemical signal. The proposed strategy combined the amplification of the HCR and the inherent redox activity of TB and utilized D-CuO/Au composites, which exhibited high sensitivity for Hg^{2+} determination. Under the optimum conditions, the proposed biosensor showed a prominent response for Hg^{2+}, including a linear range from 1 pM to 100 nM and a detection limit of 0.2 pM (S/N = 3). Moreover, the new biosensor proved its potential application for trace Hg^{2+} determination in environmental water samples.

1. Introduction

The mercuric ion (Hg^{2+}) is one of the most hazardous heavy metal contaminants that naturally occurs in the environment (Bhan and Sarkar, 2005; Wang et al., 2004). Mercury contamination is widespread in different ecological systems such as the atmosphere, soil and water (Zhang and Wong, 2007). Furthermore, even the exposure to low concentrations of mercury can cause a range of adverse health effects in humans, including neurological damage, nephrological failure, brain damage and digestive damage (Driscoll et al., 2007; Tchounwou et al., 2003). Therefore, it is essential to monitor Hg^{2+} levels. A number of traditional techniques for Hg^{2+} detection have been developed, such as atomic absorption spectrometry (Erxleben and Ruzicka, 2005; Ghaedi et al., 2006), high-performance liquid chromatography (Margetinova et al., 2008), inductively coupled plasma mass spectrometry (Long and Kelly, 2002; Tsung-Hung Lee, 2000), and the atomic emissions spectrum (Shoaee et al., 2012). However, tedious sample preparation and costly apparatuses restrict the application of these instrumental methods. Thus, it is of great importance to developing a time-saving and cost-effective method for Hg^{2+} analysis.

Thymine-Thymine (T-T) mispairs have been found that can effectively capture Hg^{2+} to form T-Hg^{2+}-T base pairs, which were proved to be more stable than the A-T pairs (Clever et al., 2007). Moreover, it has been demonstrated that the stabilizing effect of Hg^{2+} on the T-T mispairs surpasses the effects of other metal ions and appears to be highly specific (Miyake et al., 2006). With the specific T-Hg^{2+}-T complex, several electrochemical biosensors for Hg^{2+} determination have been developed (Li et al., 2010; Lv et al., 2016). Commonly, these reported biosensors exhibit good analytical performance. For instance, Tang's group designed a new 4impedimetric approach based on a nanogold-

* Correspondence to: Chongqing Medical University, Box 197#, 1 Yi Xue Yuan Road, Yuzhong District, Chongqing 400016, China.
E-mail address: hejunlin@cqmu.edu.cn (J. He).
[1] Authors contributed equally to this work.

https://doi.org/10.1016/j.bios.2019.01.063
Received 31 October 2018; Received in revised form 16 January 2019; Accepted 27 January 2019
Available online 19 February 2019
0956-5663/

functionalized dendrimer and enzyme-tyramine concatemers for the highly sensitive detection of Hg^{2+} (Qiu et al., 2016). Later, Cai et al. (2017) proposed an ultrasensitive strategy for Hg^{2+} determination using Mg^{2+}-dependent DNAzyme assisted target recycling and the hybridization chain reaction (HCR) for signal amplification. Therefore, inspired on these methods, we find that the high sensitivity of biosensors relies on a creative, effective and powerful signal amplification strategy. Thus, based on the T-Hg^{2+}-T interaction, we attempted to develop a novel electrochemical biosensor with excellent sensitivity.

To achieve an excellent amplified response signal output, the HCR is employed for the signal amplification strategy. The HCR is an initiator-triggered reaction, which uses the single-stranded DNA (ssDNA) molecule as a structural material to construct nicked double helices through self-assembly (Huang et al., 2011; Yin et al., 2008). The two stable species of DNA hairpins that the hybridization process coexist in the solution until an initiator strand is introduced (Choi et al., 2010). Moreover, the linkage of many oligonucleotides in the HCR event exhibits great potential for signal amplification. Thus, based on these advantages of the HCR, toluidine blue (TB) is employed as electron transfer mediator (Bai et al., 2014) in the design of the amplification strategy. Since TB is a phenothiazine dye that can interact with the DNA double helix via π–π stacking with DNA bases, it has high affinity (Nguyen et al., 2016). After incorporating TB into double-strand DNA in order to form a redox polymer, the increase in the electrochemical signal response depends on the nucleic acid amplification of the HCR. Relying on the TB linking mode, two DNA hairpins that are designed for the HCR can be used without any complexity labelling. Meanwhile, in order to achieve this amplification strategy, we designed two T-rich nucleic acid single strands (P1 and P2), which can be hybridized in the presence of Hg^{2+}. Moreover, the unpaired sequence of P2 was designed as an initiation chain for the HCR, which successfully triggered the HCR reaction. In this work, the combination of TB and the HCR as a signal amplification strategy in Hg^{2+} detection occurs for the first time.

The utilization of ideal materials to construct sensing platforms is also the central research topic for increasing the sensitivity of biosensors. Hierarchically structured materials have been widely employed in many fields because of their inherent large surface areas and abundant porous structures (Shopsowitz et al., 2010; Warren et al., 2008). Especially, the hierarchically porous dandelion-like CuO (D-CuO) microsphere composed of nanobelts with a rare high surface area (Zhang et al., 2012) which made it become an ideal base material. Furthermore, it can react with abundant nanomaterials such as noble metal nanoparticles to form novel nanocomposites. Gold nanoparticles (AuNPs) are a particularly effective nanomaterial in electrochemical applications due to their favourable properties of facilitating electron transfers, biocompatibility and electroconductivity (Huang et al., 2014). Therefore, the combination of the D-CuO microsphere and AuNPs as a novel nanocomposite was suitable for selection as the sensing platform's construction material due to its good electrochemical performance and providing more active sites in combination with the T-rich nucleic acid strand (Poon et al., 2010).

In this work, we design a novel and highly sensitive biosensor based on the stable structure of T-Hg^{2+}-T for the detection of Hg^{2+}. The newly prepared D-CuO/Au composite serves as an electrode surface platform to further increase the electrochemical performance and immobilize more thiol-functionalized oligonucleotide P1. Then, in the presence of Hg^{2+}, the other ssDNA P2 can hybridize with P1 to form stand-up duplex DNA strands based on the T-Hg^{2+}-T structure. In addition, a partial sequence of P2 that does not hybridize with P1 is the initiator sequence, which is employed to trigger the HCR reaction upon the two hairpin probes (H1 and H2). The successful HCR process create amount of nicked double helices copolymers that allowed a great enhancement of TB interacted into them. Thus, the electrochemical signal can be further amplified by the inherent redox ability of TB, thereby resulting in a highly sensitive Hg^{2+} detection method. In addition, Hg^{2+} determination in tap water and factory water is applied to demonstrate the application of this proposed biosensor in real samples, which may provide a great potential method for Hg^{2+} detection in the environment.

2. Experiment

2.1. Materials and reagents

Copper nitrate hydrate ($Cu(NO_3)_2{\cdot}H_2O$) was purchased from Aladdin (China, www.aladdin-e.com). Toluidine Blue (TB), tris(2-carboxyethyl) phosphine hydrochloride (TCEP) and Pluronic F127 were purchased from Sigma-Aldrich (St. Louis, MO, USA). Gold(III) chloride trihydrate ($HAuCl_4{\cdot}4H_2O$) and ammonia water ($NH_3{\cdot}H_2O$) (25%) were purchased from Aladdin (China, www.aladdin-e.com). 6-mercapto-1-hexanol (MCH) was supplied by Sigma-Aldrich. Ascorbic acid was purchased from Guangdong Guanghua Sci-Tech Co., Ltd. (Guangdong, China). Potassium ferricyanide ($K_3Fe(CN)_6$) and potassium ferrocyanide ($K_4Fe(CN)_6$) were obtained from the Beijing Chemical Reagents Company (Beijing, China). Ethylene glycol (C_2H_6O) was purchased from Chongqing Chuandong Chemical Group Co., Ltd. (Chongqing, China). The Hg^{2+} standard solution was purchased from Beijing Solarbio Science & Technology Co., Ltd. (Beijing, China).

All oligonucleotide sequences were synthesized by Sangon Biotech Co., Ltd. (Shanghai, China) and are listed as follows:

P1: 5′-HS-$(CH_2)_6$- TTTGCTCTCTCGTTT-3′,

P2: 5′- ACTCAATAGCTTTCGTGTGTGCTTT-3′,

Hairpin probe (H1): 5′- GCTATTGAGTCACAATACAG-3′, and

Hairpin probe (H2): 5′- ACTCAATAGCCTGTATTGTG-3′.

We utilize a Tris-HCl buffer 1 (10 mM Trishydroxymethylaminomethane hydrochloride (Tris-HCl), 1 mM Ethylenediaminetetraacetic acid (EDTA), 10 mM TCEP, 100 mM NaCl and 5 mM $MgCl_2$ (pH 7.4)) to dissolve the P1. A Tris-HCl buffer 2 consisting of 20 Mm Tris-HCl, 200 mM NaCl and 20 mM $MgCl_2$ (pH 7.4) was used to dissolve the P2, H1 and H2. The hairpin oligonucleotides (H1 and H2) were obtained by heating the solution at 95 °C for 5 min, and then slowly cooling it down to room temperature for at least 2 h. All other chemicals were analytical reagents and were used without further purification. Ultrapure water (> 18.2 MΩ cm) was utilized in all preparations.

2.2. Apparatus and measurements

All electrochemical analyses were carried out using a Metrohm PGSTAT 302 N workstation and a conventional three-electrode system. The field emission scanning electron microscopy (FE-SEM) was conducted using an Oxford X-max50 microscope (Oxford, England). The X-ray photoelectron spectroscopy (XPS) was conducted using a VG Scientific ESCALAB 250 spectrometer (Thermoelectricity Instruments, USA). The energy dispersive X-ray spectroscopy (EDS) patterns and Elemental mapping were collected using an Oxford X-max50 microscope. Transmission electron microscopy (TEM, Hitachi-7500158) was conducted to obtain images. The UV–vis absorption spectroscopy was recorded using a UV-2450 spectrophotometer (Shimazu, Japan). A Zetasizer Nano ZS (ZEN 3600, Malvern Instruments Ltd., UK) was utilized to analyse the Zeta potential measurements. The porous nature of the nanomaterials was determined according physical adsorption of N2 at −196 °C using the MicroActive software and an ASAP 2460.

2.3. Synthesis of dandelion-like CuO microspheres

The D-CuO microspheres were synthesized using a hydrothermal method (Zhang et al., 2012). Briefly, 2 g $Cu(NO_3)_2{\cdot}H_2O$ was dissolved in 80 mL C_2H_6O. Then, 60 mL NH4OH (25%) and 20 mL NaOH (1 mol L^{-1}) were added. After the resulting mixed solution was stirred for 20 min, a clear solution formed, which was sealed and heated on a hot plate at 130 °C for 12 h, and then cooled down to room temperature.

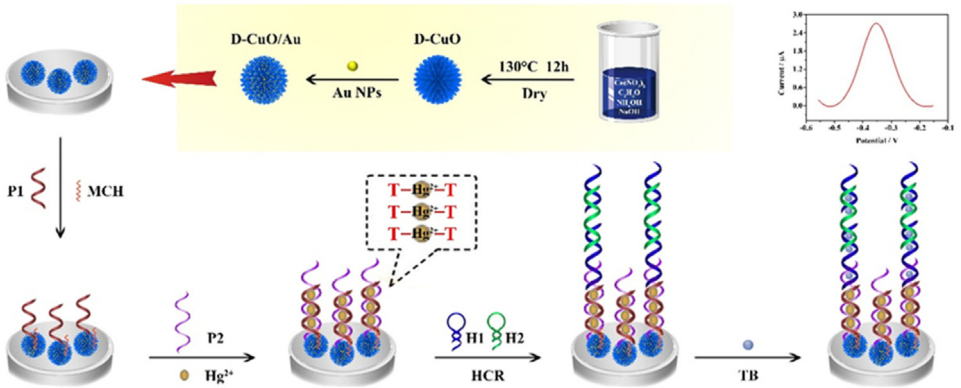

Scheme 1. Schematic representation of the biosensor for the Hg^{2+} determination.

The obtained solid precipitate was purified using centrifugation and washed three times with ultrapure water. Finally, it was dried on a hot plate at 90 °C for 8 h.

2.4. Synthesis of Au nanoparticles and D-CuO/Au nanocomposites

Au nanoparticles (Au NPs) were synthesized using the one-pot method (Wang and Yamauchi, 2010). First, 0.01 g Pluronic F127 was dissolved in 1 mL $HAuCl_4 \cdot 4H_2O$ under constant stirring. Then, 1 mL AA (0.4 mol L^{-1}) was added into the obtained solution. After the mixture was stirred at 600 rpm for 3 h, the products were centrifuged at 12,000 rpm for 20 min and washed with ultrapure water three times. The Au NPs was dispersed into 1 mL ultrapure water. The D-CuO/Au was synthesized as follows. Briefly, 2 mg D-CuO was added into 1 mL ultrapure water and sonicated. After the Au NP solution was injected under vigorous stirring at 80 °C for 30 min, then the D-CuO/Au nanocomposites formed.

2.5. Preparation of electrochemical biosensor

Scheme 1 illustrates the fabrication process of the biosensor. Prior to use, GCE was thoroughly polished with 0.3 and 0.05 μm alumina slurries until a mirror-like surface was achieved. Then, the electrode was sonicated in ultrapure water, ethanol and ultrapure water for 5 min. Then, 10 μL CuO-Au composites were modified onto the electrode and allowed to dry at room temperature. Successively, 10 μL 2 μM P1 was dropped on the electrode surface for 2 h at 37 °C. Next, 10 μL 100 μM MCH was attached onto the electrode surface for 30 min to eliminate nonspecific binding effects and block the remaining active groups. The prepared electrode was further incubated with a mixture of 20 μL P2

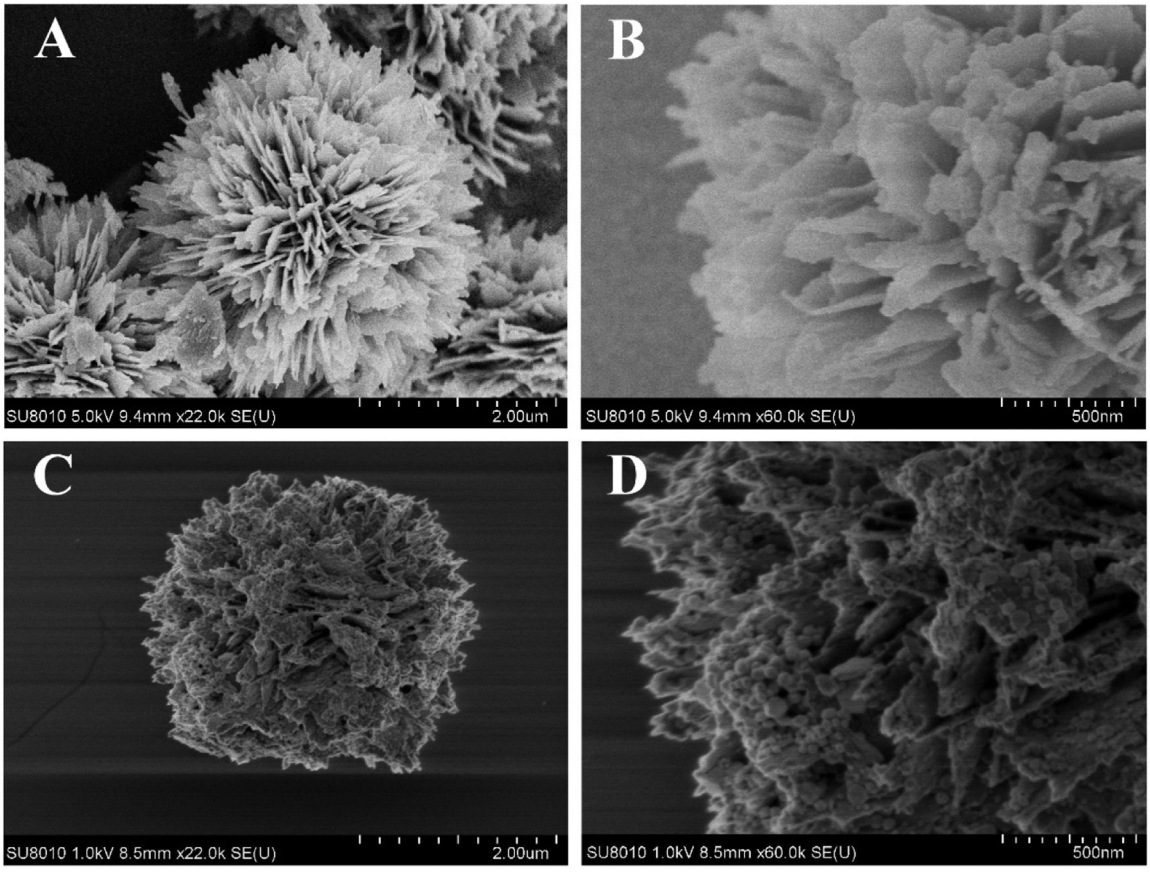

Fig. 1. FE-SEM images of D-CuO (A); the magnified views of D-CuO (B), and D-CuO/Au (C); and the magnified views of D-CuO/Au (D).

(2 μM) and Hg^{2+} of different concentrations for 1 h at room temperature. Subsequently, a mixture of 20 μL hairpin probes H1 and H2 was incubated on the modified electrode for 2 h at 37 °C. Finally, the electrode was immersed into a TB solution (0.02 mM TB, 0.2 M NaCl, 0.10 M PBS pH 7.4) for 5 min. The resulting electrode was carefully rinsed with ultrapure water to remove any excess TB and the electrochemical signal was recorded using differential pulse voltammetry (DPV) in 0.1 M PBS (pH 7.4).

3. Results and discussion

3.1. Characterization of D-CuO microspheres and D-CuO/Au composites

Fig. 1A shows the FE-SEM image of the synthesized D-CuO microspheres. It can be shown that the D-CuO microspheres exhibit a dandelion-like porous structure with an average diameter of 2 μm. As shown in the magnified image of D-CuO (Fig. 1B), the D-CuO microspheres consist of a large number of thin nanosheets that are projected from the core. Moreover, the N_2 adsorption-desorption isotherm that is presented in Fig. S1 shows that the D-CuO microspheres's BET surface area is 12.6119 m^2/g, and the inset of Fig. S1 demonstrated the presence of a porous structure for D-CuO microspheres. The morphology of the D-CuO/Au composites was displayed in Fig. 1C, where the interstices of the D-CuO microspheres were evenly decorated with pellet-shaped AuNPs. In addition, the magnified image (Fig. 1D) shows that the AuNPs have a size of approximately 50 nm. Furthermore, TEM was used to determine the successfully synthesized D-CuO microspheres and D-CuO/Au composites. The result is given in the supplementary information (Fig. S2).

Detailed XPS analysis was used to demonstrate chemical states of the D-CuO/Au composites, and the results are shown in Fig. 2A-D. The Cu 2p and O 1 s peaks were assigned to the D-CuO microspheres and the Au 4 f peaks corresponded to the AuNPs (Fig. 2A). In Fig. 2B, the XPS spectra taken from the Cu 2p region of the D-CuO/Au composites, which peaks at 933.58 eV, was attributed to the core level of Cu 2p (Anandan et al., 2012). The O 1 s region peak at 532.08 eV can be assigned to the O (-2) in the D-CuO/Au composites (Fig. 2C) (Ghijsen et al., 1988). Fig. 2D displayed the Au 4f region peaks at 83.88 eV, which correspond to the Au (0) in the D-CuO/Au composites (Chang et al., 2006). Additionally, the EDS image showed the existence of Cu, O and Au elements (Fig. 2E). Clearly, the elemental mapping indicated that Cu, O and Au are uniformly distributed throughout the D-CuO/Au composites (Fig. 2F-H). In addition, the UV–Vis absorption spectra and the zeta potential were illustrated in Fig. S2. Compared with CuO, D-CuO/Au exhibited an absorption peak at 560 nm, indicating that AuNPs were successfully modified on the D-CuO microspheres (Fig. S3A) (Yu et al., 2014). Meanwhile, the zeta potential of D-CuO, AuNPs and D-CuO/Au were −8.79, −10.82 and −14.77, respectively (Fig. S3B). All the results suggested that the D-CuO/Au composites had been successfully synthesized.

3.2. Feasibility testing of the strategy

3.2.1. Agarose gel electrophoresis analysis

To confirm the feasibility of the biosensor for Hg^{2+} determination based on the T-Hg^{2+}-T institution and the HCR amplification strategy, agarose gel electrophoresis was applied to characterize the different samples. As shown in Fig. S4, two T-rich oligonucleotides that consist of P1 and P2 were shown in Lane 1 and Lane 2, respectively. Compared with P1 and P2, the mixed solution of the target Hg^{2+}, P1 and P2 had lower mobility, which reflected the successful hybridization of P1 and P2 based on the T-Hg^{2+}-T base pair. Subsequently, Lane 4 and Lane 5 have no significant difference due to the identical base numbers of H1 and H2. After the mixture of P2, H1 and H2, some obvious bands were observed at the bottom with much slower migration (Lane 6) (Chen et al., 2012; Xu et al., 2017), thus suggesting that P2 can trigger the HCR to form a long double-strand DNA. As expected, these results reflected the successful production of the T-Hg^{2+}-T complex and the HCR reaction.

3.2.2. DPV analysis

The DPV was also utilized to investigate the feasibility of the biosensor for Hg^{2+} determination. Fig. 3B shows that the signal responses of the reduction reaction of TB can be intercalators in double-stranded DNA under different experimental conditions. Without Hg^{2+}, a tiny reduction current was obtained (curve a), which can probably be attributed to the TB that can also interacted with the small groove of the single strand DNA through hydrophobic effect (Peng et al., 2015; Tavallaie et al., 2014) and the nonspecific adsorption. When Hg^{2+} and H1 were introduced, the current response (curve b) had no significant increase compared to the blank. Otherwise, in the absence of H1, a small current peak was observed (curve c) when H2 was introduced to

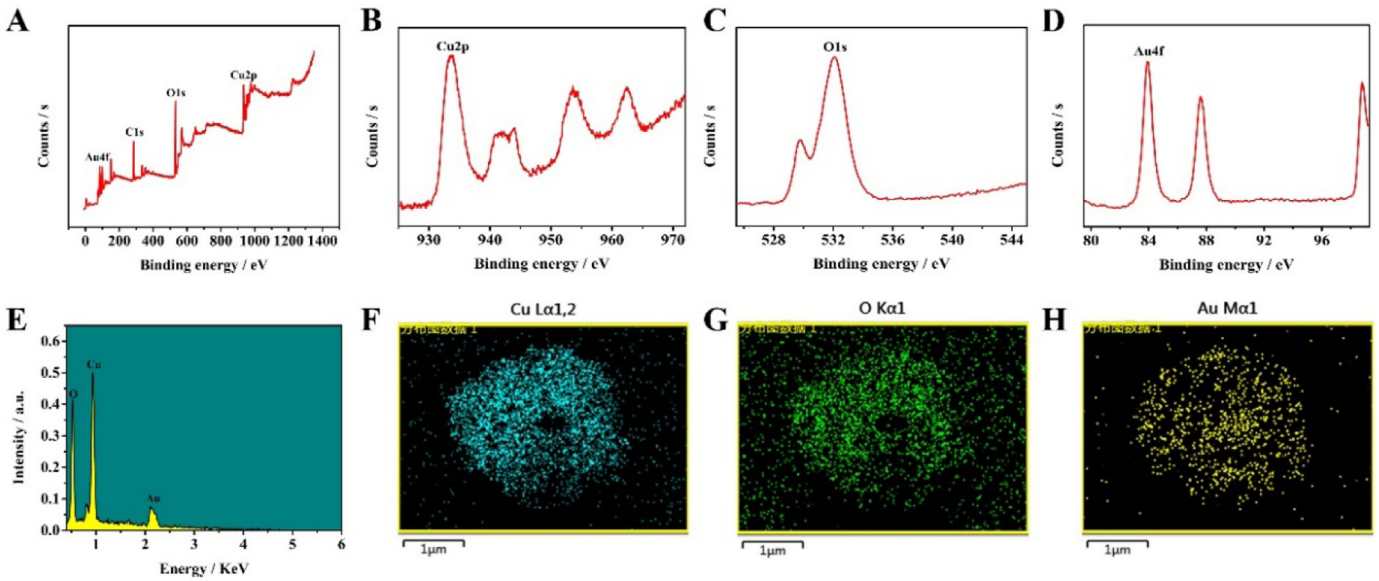

Fig. 2. The XPS spectra of D-CuO/Au (A). (B) Cu 2p, (C) O 1s, and (D) Au 4f signals derived from D-CuO/Au. (E) EDS spectrum and Elemental mapping of D-CuO containing Cu (F), O (G), and Au (H).

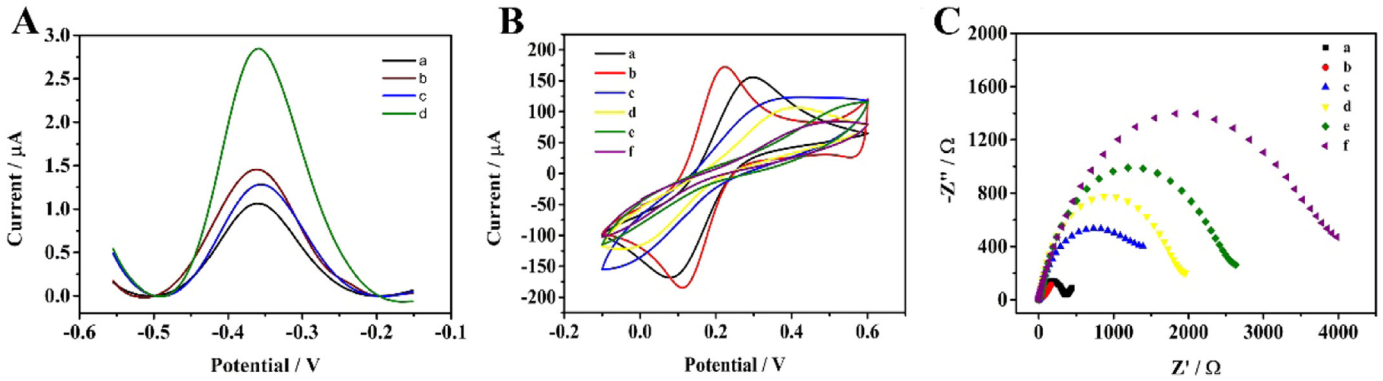

Fig. 3. (A) DPV curves of different modified electrodes: (a) D-CuO/Au + P1 + MCH + P2 + H1 + H2 + TB, (b) D-CuO/Au + P1 + MCH + Hg^{2+} + P2 + H1 + TB, (c) D-CuO/Au + P1 + MCH + Hg^{2+} + P2 + H2 + TB, and (d) D-CuO/Au + P1 + MCH + Hg^{2+} + P2 + H1 + H2 + TB. (B) CV and (C) EIS characterizations of the modified electrode responses: (a) bare GCE, (b) D-CuO/Au/GCE, (c) P1/D-CuO/Au/GCE, (d) MCH/P1/D-CuO/Au/GCE, (e) d incubated with the mixture of 2 μM P2 and 10 nM Hg^{2+}, and (f) e incubated with 2.0 μM H1 and 2.0 μM H2.

the HCR reaction, even in the presence of Hg^{2+}. From the result of the HCR signal amplification, curve d showed an obvious current peak when the HCR process was completed, which revealed that it is an efficient signal amplification strategy for this biosensor.

3.3. Characterization of the stepwise-modified biosensor

Cyclic voltammetry (CV) measurements were utilized to characterize the interface properties of the surface-modified electrodes. Fig. 3C illustrated the CV of the different modified electrodes that were obtained in a 5 mM $[Fe(CN)_6]^{3-/4-}$ solution containing 0.1 M KCL. The D-CuO/Au-modified GCE electrode (curve b) had an increased current redox peak over the bare GCE (curve a), which is attributed to D-CuO/Au and can promote the electron transfer. After the thiolated probe P1 was immobilized on the electrode surface through forming an Au—S bond, the current peak decreased remarkably (curve c) because of the abundant negatively charged DNA backbones that hinder electron transfer. Then, non-conductive MCH was employed to block unoccupied sites, and the current peak correspondingly declined (curve d). When the electrode was incubated with P2 and Hg^{2+}, the current redox peak further decreased (curve e) because of the hybridization reaction between P1 and P2 from forming T-Hg^{2+}-T base pairs. Subsequently, a decreased peak current was observed (curve f) after incubating with H1 and H2 for the HCR, thus indicating that the double helices copolymers of oligonucleotide probes can significantly block the electron transfer.

The fabrication process of the biosensor can also be assessed using electrochemical impedance spectroscopy (EIS). As shown in Fig. 3D, the bare GCE exhibited a small semicircle domain because of a relatively low resistance (curve a). After the electrode was modified with D-CuO/Au, the resistance decreased (curve b) as the D-CuO/Au on the GCE surface accelerated the electron transfer. The resistance increased significantly (curve c) after the modified electrode was incubated with the thiolated probe P1 due to their non-electroactive property. Successively, when the electrode was blocked by the non-conductive MCH, the resistance remained increased (curve d). After assembling P2 and Hg^{2+} on the electrode surface, the resistance is further increased (curve e), which is attributed to the hybridization of P1 and P2 via T–Hg^{2+}–T complexes. When the electrode was incubated with H1 and H2 for the HCR strategy, a large increased semicircle domain (curve f) was observed. The above results verified the successful fabrication of the biosensor.

3.4. Optimization of the experimental conditions

To acquire the optimum sensing performance, some crucial parameters were investigated such as the volume of D-CuO/Au, the concentration of the thiolated probe P1, the immobilization time of the thiolated probe P1 and the hybridization time between P1 and P2 through the T–Hg^{2+}–T structure. As shown in Fig. S5A, the current change increased remarkably until the volume of D-CuO/Au increased to 10 μL. Then, the current slowly decreased from 10 μL to 14 μL. Therefore, 10 μL was selected as the optimum concentration of D-CuO/Au for the test.

In addition, the immobilization of the thiolated probe P1 on the electrode surface was a crucial step for the performance of the biosensor. The immobilization time and the concentration of the thiolated probe P1 were optimized. As shown in Fig. S5B, it is apparent that the current change increased as the incubation time increased and appears to remain steady when the time was 120 min. Thus, the optimum immobilization of the thiolated probe P1 was 120 min. Furthermore, the current response increased from 1.0 μM to 2.0 μM and subsequently approached a plateau (Fig. S5C), thereby indicating the maximum concentration of the thiolated probe P1 was obtained. Thus, the optimal concentration of P1 was determined to be 2.0 μM.

The efficiency of the proposed biosensor also depended on the hybridization time between P1 and P2 in the presence of Hg^{2+}. As the hybridization time increased, the current change first increased and then reached maximum at 60 min (Fig. S5D). The result suggested that the hybridization reaction between P1 and P2 in the presence of Hg^{2+} was completed after 60 min. Hence, 60 min was employed as the hybridization time in this experiment.

3.5. Analytical performance of the biosensor

The performance of the proposed biosensor was assessed using DPV under the optimal experimental conditions. It can be clearly seen that the current response increased gradually with the increase of the Hg^{2+} concentration (Fig. 4A). The current peaks were attributed to the oxidation of TB, which were linearly proportional to the logarithm of the Hg^{2+} concentration. Furthermore, a linear correlation was found in the range of 0.001–100 nM (Fig. 4B), which followed the regression equation of $Y = 0.26825*\log C_{Hg^{2+}} + 1.5956$ (Y is the DPV current peak, $C_{Hg^{2+}}$ is the concentration of Hg^{2+} and $R^2 = 0.9983$). The detection limit (DL) was calculated to be 0.2 pM ($DL = 3S_B/m$, where S_B is the standard deviation of the blank, and m is the slope of the calibration curve). In addition, compared with other reported methods in the literature, which were shown in Table S1, the proposed biosensor was more sensitive and had a lower detection limit due to the employment of the HCR that significantly enhanced the current response.

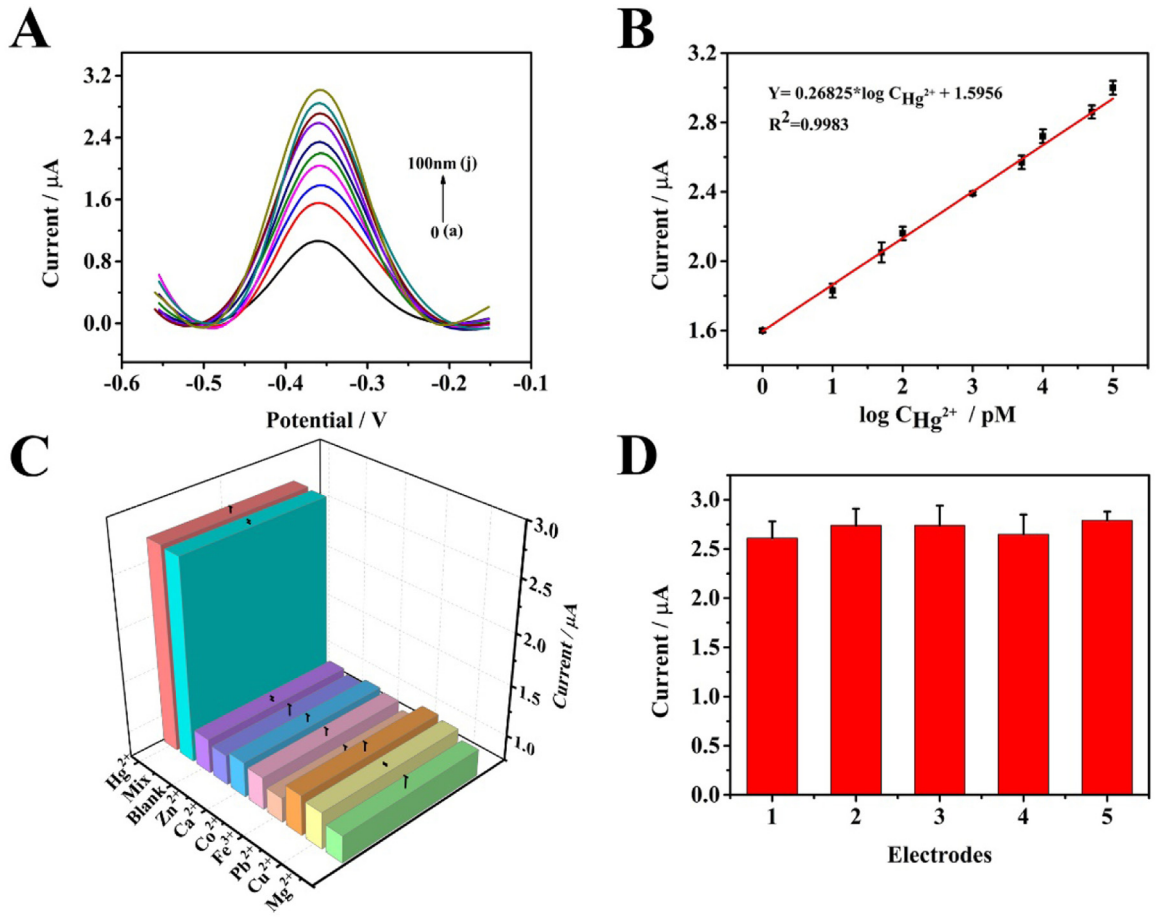

Fig. 4. (A) DPV curve responses of the proposed biosensor assay with different Hg^{2+} concentrations: (a) 0 pM, (b) 1 pM, (c) 10 pM, (d) 50 pM, (e) 100 pM, (f) 1 nM, (g) 5 nM, (h) 10 nM, (i) 50 nM, and (j) 100 nM. (B) The linear relationship between the electrochemical responses and the different Hg^{2+} concentrations (n = 3). (C) The responses of the proposed biosensor to other metal ions (Zn^{2+}, Ca^{2+}, Co^{2+}, Fe^{3+}, Pb^{2+}, Cu^{2+}, and Mg^{2+}) (1.0 μM), a mixture (Mix) of metal ions (1.0 μM) and Hg^{2+} (10.0 nM) and zero analyte (Blank). (D) The reproducibility of the five modified electrodes for the detection of 10 nM Hg^{2+}.

Table 1
Recovery of Hg^{2+} in aqueous samples.

Sample	Added Hg^{2+} (pM)	Founded Hg^{2+} (pM)	RSD (%, n = 3)	Recovery (%, n = 3)
	0	N		
	100	100.4	3.32	100.40
Tap water	1000	958.4	0.11	95.84
	10,000	10,129.6	3.10	101.30
	0	N		
	100	100.1	2.60	100.10
Factory water	1000	1027.4	3.99	102.74
	10,000	10,492.4	1.97	104.92

N: Not available.

3.6. Specificity, stability and reproducibility of the biosensor

To investigate the specificity of the proposed biosensor, several possible interfering ions were tested, such as Zn^{2+}, Ca^{2+}, Co^{2+}, Fe^{3+}, Pb^{2+}, Cu^{2+}, and Mg^{2+}. As seen from Fig. 4C, similar with the blank assay, no significant changes in the current response were obtained for these other ions at the 100-fold Hg^{2+} concentration (1 μM) alone. However, the presence of Hg^{2+} (10 nM) resulted in a significant increase in the current. Moreover, the current response of the mixture (Mix) (consisting of the 7 interfering ions (1 μM) and 10 nM Hg^{2+}) indicated that the interfering ions do not obviously affect the current change. The results demonstrated that the biosensor showed excellent specificity towards Hg^{2+} for the T–Hg^{2+}–T structure.

The long-term stability of the biosensor was tested by storing the prepared biosensor at 4 °C and measuring it every 7 days. After the fabricated biosensor was stored for 21 days, the current response remained at 92.6% of its initial values (Fig. S6). The results demonstrated that the proposed biosensor had satisfactory stability. Furthermore, the reproducibility of the biosensor was estimated by analysing the same concentration of Hg^{2+} (10 nM) using five prepared electrodes under the same experimental stages (Fig. 4D). A relative standard deviation (RSD) of 3.27% was acquired, which demonstrated its good reproducibility.

3.7. Analysis using real water samples

To evaluate the practical application of the manufactured biosensor, recovery experiments were carried out using standard addition methods in tap water samples and factory samples. A series of water samples were prepared that were spiked different Hg^{2+} concentrations (100 pM, 1000 pM, and 10,000 pM). Then, the biosensors were applied to analyse the obtained samples and the results were listed in Table 1. The recovery rates were between 95.84% and 101.30% and the relative standard deviations were from 0.11% to 3.99%. All results indicated that the fabricated biosensor provided a promising potential application for environmental water samples.

4. Conclusion

In general, we have successfully developed a highly sensitive and selective electrochemical biosensor for Hg^{2+} determination, which uses

TB both as a trace indicator and for redox activities enhancement. The utilization of D-CuO/Au composites and the HCR strategy for signal amplification can further promote the sensitivity of the manufactured biosensor. This paradigm takes advantage of the structure of long nicked double helices. Abundant TB can attach to the double strands via π–π stacking with DNA bases, thus resulting in an amplified electrochemical response of TB. Furthermore, the specificity of the proposed biosensor was guaranteed by the specific T-Hg^{2+}-T base pair, which can distinguish Hg^{2+} from other interference metal ions. Additionally, the fabricated biosensor has promising potential for Hg^{2+} in complex water samples, which was demonstrated by the recovery experiments. We believe that this strategy also showed good potential for other specific targets by simply changing the sequences of the oligonucleotides. However, we cannot find enough contaminated water samples to further prove the application of this biosensor in the environment. Thus, future work needs to continue improving in this aspect. Moreover, we will attempt to explore the application of other aromatic heterocyclic dye in our signal amplification strategy.

Acknowledgements

We are grateful for the financial support from the National Natural Science Foundation of China (No. 31571554) and the Outstanding Graduate Student Cultivation Program of Chongqing Medical University (No. BJRC201722)

Author declaration

None declared.

Appendix A. Supporting information

Supplementary data associated with this article can be found in the online version at doi:10.1016/j.bios.2019.01.063.

References

Anandan, S., Lee, G.J., Wu, J.J., 2012. Ultrason. Sonochem. 19, 682–686.
Bai, L., Chai, Y., Pu, X., Yuan, R., 2014. Nanoscale 6, 2902–2908.
Bhan, A., Sarkar, N.N., 2005. Rev. Environ. Health 20, 39–56.
Cai, W., Xie, S., Zhang, J., Tang, D., Tang, Y., 2017. Biosens. Bioelectron. 98, 466–472.
Chang, F.W., Yu, H.Y., Roselin, L.S., Yang, H.C., Ou, T.C., 2006. Appl. Catal. A General. 302, 157–167.
Chen, Y., Xu, J., Su, J., Xiang, Y., Yuan, R., Chai, Y., 2012. Anal. Chem. 84, 7750–7755.
Choi, H.M.T., Chang, J.Y., Le, A.T., Padilla, J.E., Fraser, S.E., Pierce, N.A., 2010. Nat. Biotechnol. 28, 1208–1212.
Clever, G.H., Kaul, C., Carell, T., 2007. Angew. Chem. Int. Ed. Engl. 46, 6226–6236.
Driscoll, C.T., Han, Y.-J., Chen, C.Y., Evers, D.C., Lambert, K.F., Holsen, T.M., Kamman, N.C., Munson, R.K., 2007. BioScience 57, 17–28.
Erxleben, H., Ruzicka, J., 2005. Anal. Chem. 77, 5124–5128.
Ghaedi, M., Reza Fathi, M., Shokrollahi, A., Shajarat, F., 2006. Anal. Lett. 39, 1171–1185.
Ghijsen, J., Tjeng, L.H., Elp, J.V., Eskes, H., Westerink, J., Sawatzky, G.A., Czyzyk, M.T., 1988. Phys. Rev. b 38, 11322.
Huang, J., Wu, Y., Chen, Y., Zhu, Z., Yang, X., Yang, C.J., Wang, K., Tan, W., 2011. Angew. Chem. Int. Ed. Engl. 123, 421–424.
Huang, K.J., Liu, Y.J., Liu, Y.M., Wang, L.L., 2014. J. Hazard. Mater. 276, 207–215.
Li, Q., Zhou, X., Xing, D., 2010. Biosens. Bioelectron. 26, 859–862.
Long, S.E., Kelly, W.R., 2002. Anal. Chem. 74, 1477–1483.
Lv, Y., Yang, L., Mao, X., Lu, M., Zhao, J., Yin, Y., 2016. Biosens. Bioelectron. 85, 664–668.
Margetinova, J., Houserova-Pelcova, P., Kuban, V., 2008. Anal. Chim. Acta 615, 115–123.
Miyake, Y., Togashi, H., Tashiro, M., Yamaguchi, H., Oda, S., Kudo, M., Tanaka, Y., Kondo, Y., Sawa, R., Fujimoto, T., Machinami, T., Ono, A., 2006. J. Am. Chem. Soc. 128, 2172–2173.
Nguyen, K.V., Holade, Y., Minteer, S.D., 2016. ACS Catal. 6, 2603–2607.
Peng, H.P., Hu, Y., Liu, P., Deng, Y.N., Wang, P., Chen, W., Liu, A.L., Chen, Y.Z., Lin, X.H., 2015. Sens. Actuators B Chem. 207, 269–276.
Poon, L., Zandberg, W., Hsiao, D., Erno, Z., Sen, D., Gates, B.D., Branda, N.R., 2010. Acs Nano 4, 6395.
Qiu, Z., Tang, D., Shu, J., Chen, G., Tang, D., 2016. Biosens. Bioelectron. 75, 108–115.
Shoaee, H., Roshdi, M., Khanlarzadeh, N., Beiraghi, A., 2012. Spectrochim. Acta A Mol. Biomol. Spectrosc. 98, 70–75.
Shopsowitz, K.E., Qi, H., Hamad, W.Y., Maclachlan, M.J., 2010. Nature 468, 422–425.
Tavallaie, R., Darwish, N., Gebala, M., Hibbert, D.B., Gooding, J.J., 2014. Chemelectrochem 1, 165–171.
Tchounwou, P.B., Ayensu, W.K., Ninashvili, N., Sutton, D., 2003. Environ. Toxicol. 18, 149–175.
Tsung-Hung Lee, S.-J.J., 2000. Anal. Chim. Acta 413, 197–205.
Wang, L., Yamauchi, Y., 2010. Chem. Asian J. 5, 2493–2498.
Wang, Q., Kim, D., Dionysiou, D.D., Sorial, G.A., Timberlake, D., 2004. Environ. Pollut. 131, 323–336.
Warren, S.C., Messina, L.C., Slaughter, L.S., Kamperman, M., Zhou, Q., Gruner, S.M., Disalvo, F.J., Wiesner, U., 2008. Science 320, 1748–1752.
Xu, W., Tian, J., Shao, X., Zhu, L., Huang, K., Luo, Y., 2017. Biosens. Bioelectron. 89, 795–801.
Yin, P., Choi, H.M.T., Calvert, C.R., Pierce, N.A., 2008. Nature 451, 318–322.
Yu, R., Shibayama, T., Meng, X., Takayanagi, S., Yoshida, Y., Yatsu, S., Watanabe, S., 2014. Appl. Surf. Sci. 289, 274–280.
Zhang, L., Wong, M.H., 2007. Environ. Int. 33, 108–121.
Zhang, Z., Che, H., Wang, Y., Song, L., Zhong, Z., Su, F., 2012. Catal. Sci. Technol. 2, 1953.